Development of a mobile powered hole digger for orchard tree cultivation using a slider-crank feed mechanism

Zong Wangyuan[1], Wang Jingliang[1], Huang Xiaomao[1,2],
Yu Dong[1], Zhao Yingbiao[1], Sean Graham[1]

(1. *College of Engineering, Huazhong Agricultural University, Wuhan 430070, China*;
2. *Department of Agricultural and Biosystems Engineering, Iowa State University, Ames, IA 50011, USA*)

Abstract: The powered hole digger is one of the most important orchard machines.   The power consumption of its drill is an important factor affecting the performance and operation of the device.   The drill power consumption of the digger at a constant feed rate is directly proportional to digging depth.   This research discusses a newly designed powered hole digger using a slider-crank feed mechanism.   The motion characteristics of the powered hole digger feeding mechanism was analysed. Additionally, an experiment was conducted to determine the characteristics of the drill power consumption.   It can be concluded that there was a positive correlation between the drill power consumption and the powered hole digger feed rate.   It was observed that when digging depth reached 200 mm, the drill power consumption reached the maximum power rating; subsequently the drill power consumption decreased with an increase of digging depth.   When the drill reached the bottom of the hole, the power consumption of the new powered hole digger did not exceed the maximum designed power rating, hence the drill motor would not stall.

Keywords: powered hole digger, crank-slider, drill power consumption, orchard tree

1   Introduction

The powered hole digger plays an important role in

orchard machinery due to its applications in transplanting fruit tree seedlings, fruit tree fertilization and occasionally for burying piles[1].

Research related to powered hole digger is limited. Kathirvel et al.[2] developed an auger digger as attachment to a power tiller, digging 35-40 holes per hour with diameter of 22.5 cm and depth of 45 cm.   Singh[3] studied the performance of the tree planting powered hole digger mounted to a tractor.   Purtskhvanidze et al.[4] developed a powered hole digger which can work on sloped surfaces, with low power consumption and improved mobility.   Wang et al.[5] measured the mechanical parameters during the digging operations using a computerized data acquisition system with electrical sensors in real-time mode, and studied the relationship between the job parameters (drill speed, feed rate) and the drill dynamic parameters (torque, feed resistance) and obtained the corresponding fitting equation.   Ma[6] proposed a method for using the drill's

resistance and the natural frequency of the linkage to control the trajectory of the drill. It deduced the natural frequency of the elastic digging linkage mechanism in general, and produced a calculation program outlining the drill trajectory when only the cylinder's push speed was changed while other conditions remain constant. From the perspective of system dynamics, Meng et al.[7] set up the dynamic model of systems with the drill of a deep hole digger, the soil based on wave theory and finite element method and solved the equation by numerical methods. Yang et al.[8,9] studied the bending and torsion vibration of the tractor-mounted diggers using power analysis and dynamic design method, and obtained the system's natural frequency and main vibration mode. Macphersonet al.[10] established the longitudinal torsion vibration model of a drill rod with wave theory, and compared to the actual measurement results. Brakel et al.[11] established a finite element model of the drill's instantaneous power using three-dimensional linear beam elements, solved the dynamic finite element equations with the Wilson-9 law and Gaussian elimination method, and determined the contact force caused by the imposed constraints of hole wall with New-Raphson iteration method. Altintas et al.[12-15] established mechanics and dynamics model of various shaped helix drills. This model can be used to predict the stability during drilling.

Currently, there are very few researches on analyzing the drill power consumption of powered hole diggers. The drill power consumption of the commonly used powered hole digger with constant feed rate increases with the increasing digging depth (h), this results in the powered hole digger stalling when the power of its motor exceeds the maximum designed power rating.

This research proposes a solution to this problem by using a newly designed powered hole digger with a slider-crank feed mechanism. This method is based on the soil transport theory. The motion characteristics of the powered hole digger feeding mechanism was analyzed; Additionally an experiment was conducted for observing the power consumption characteristics of the digger's drill. It was observed that there is a positive correlation between the drill power consumption and the powered hole digger's feed rate.

2   Design of the powered hole diggers and analysis of the motion characteristics of the feeding mechanism.

2.1   Design of the slider-crank feed mechanism

2.1.1   Determination of the crank length

The new powered hole digger will be used for fertilization in the persimmon garden. The depth of the hole which was dug by the now powered hole digger was 0.3 m according to the manuring requirements. The distance between the powered hole digger's drill and ground was greater than 0.2 m according to the moving requirements; therefore the length of crank given for this consideration should be 0.3 m.

2.1.2   Determination of the rocker length

When the length of crank was determined, the length of rocker decided the speed characteristics of the slider. But the soil transport effect was affected by the speed characteristics of the slider. So in order to determine the length of rocker, the relationship between the length of rocker and slider speed should be found. Then the length of rocker will be determined according to the soil transport theory.

The slider-crank mechanism movement diagram is shown in Figure 1. AB is the rocker, with length of b, BC is the crank, with length of a, C is the slider. The angle between AB and the vertical line is θ; The angle between BC and the vertical line is β. Timing is started when C is at its highest position.
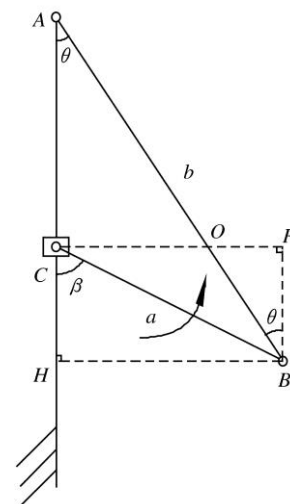

Figure 1   Feed mechanism motion sketch

The instantaneous velocity center of BC can be

determined using plotting methods.   Lines though B that are perpendicular to CO and AC can be drawn and the respective intersection points are denoted P and H.   This operation can result in a rectangular CPBH with CP=HB and CH=PB.   The following equations are subsequently obtained according to the above geometric relations:

$$CO = PC - PO = HB - PO$$
$$= a\sin\beta - a\cos\beta\tan\theta$$

and $\sin\theta = \dfrac{a\sin\beta}{b}$

then,

$$CO = a\sin\beta - a\cos\beta\sqrt{\dfrac{a^2\sin^2\beta}{b^2 - a^2\sin^2\beta}}$$
$$= a\sin\beta - \dfrac{a^2\cos\beta\sin\beta}{\sqrt{b^2 - a^2\sin^2\beta}} \tag{1}$$

As can be seen from Equation (1) that CO is a binary function which has two arguments (β and b) while keeping (a) constant.   A study of the variation of CO was carried out.   The values of b (m) are [0.35, 0.40, 0.45, 0.50, 0.55, 0.60, 0.65, 0.70, 0.75, 0.80, 0.85, 0.90, 0.95, 1.00].   The values of β ($°$) are [0, 1, 2, 3, 4, 5, 6, 7, ···, 180].   Each value of b and β is taken into Equation (1).   When the b is constant, β takes every value, seeking maximum value of CO.   The maximum value of CO is shown in Table 1.

Table 1   The maximum value of CO corresponded to each rocker length

Length of rocker/m	Max of instant heart radius/m	β/($°$)
0.35	0.42855	116
0.40	0.38966	116
0.45	0.36807	116
0.50	0.35404	115
0.55	0.34421	113
0.60	0.33695	112
0.65	0.33141	111
0.70	0.32705	110
0.75	0.32356	109
0.80	0.32071	108
0.85	0.31835	108
0.90	0.31639	107
0.95	0.31472	106
1.00	0.31329	105

Substituting the maximum instantaneous velocity center radius into Equation (2) to obtain the maximum value of slider feed speed.

$$V_s = l_{co}\omega_q \tag{2}$$

where, V_s is slider feed speed (drill feed speed), m/s; l_{co} is instantaneous velocity center radius (CO), m; ω_q is crank speed, rad/s.

According to Equation (2), when the value of ω_q is unchanged V_s and l_{co} reached the maximum at the same time.   According to the soil transport theory[1], if the soil vertical speed (V_z) is greater than 0 then the soil will be transported up.   According to Equation (3), V_s and the soil vertical speed (V_z) reached the maximum at the same time.   Hence when the value of ω_q is fixed, if l_{co} reached the maximum (V_z reached the maximum) the soil vertical speed is greater than 0 then all values of l_{co} meet the requirements.

The soil vertical speed:

$$V_z = \dfrac{r_0\omega b}{2pc}\left[AB - \sqrt{(AB)^2 - 4P\left(A^2 a - \dfrac{E}{f_2}\right)}\right] \tag{3}$$

where: r_0 is drill radius, m; ω is drill rotational speed, rad/s; b is coefficient, $b=\cot(\alpha+\varphi_1)$; c is soil speed coefficient; α is rise angle of the drill, ($°$); φ_1 is friction angle between soil and steel, ($°$); φ_2 soil internal friction angle, ($°$); f_2 is soil internal friction coefficient, $f_2=\tan\varphi_2$; ξ is the angle between soil particle velocity and horizontal plane, ($°$), $\tan\xi = \dfrac{V_s}{r\omega_0}$; A, B, P, E are coefficients,

$A = 1 - \dfrac{\tan\xi}{\tan\alpha}$, $B = a + 2b + 0.4ab$,

$P = b(1 + 0.4a + 0.4b + 0.16ab) + b$, $E = \dfrac{g}{r_0\omega^2}$;

when $E \leqq 0.025$, $c = 1$

when $E \leqq 1.1$, $c = \dfrac{0.6\sin(2\alpha + 8°)}{th\dfrac{0.02}{E}}$

when $E > 1.1$, $c = \dfrac{1.1\sin(2\alpha + 8°)}{th\dfrac{0.05}{E}}$

For the new powered hole digger: the drill radius (r_0) is 0.05 m; the rise angle of the drill (α) is 20$°$; the reduction ratio (ω: ω_q) is 90:1.

According to the relevant documents[1]: the friction angle between soil and steel (φ_1) is 20$°$; the soil internal friction angle (φ_2) is 30$°$.

Since the drill rotational speed can be adjusted within a certain range (350-400 r/min), the values of drill rotational speed (r/min) are [350, 355, 360, 365, 370, 375, 380, 385, 390, 395, 340].   Table 2 presents the results of substituting the drill rotational speed (ω) and each rocker value (Table 1) into Equation (3) to obtain.

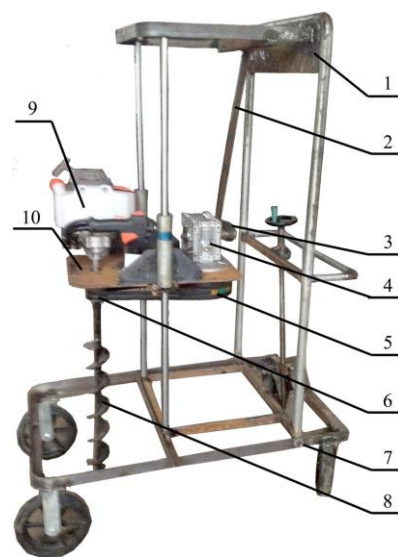**Table 2   Soil vertical speed**   m s^{-1}

Rocker length/m	Drill rotational speed/r·min^{-1}										
	350	355	360	365	370	375	380	385	390	395	400
0.35	−0.0154	−0.0140	−0.0126	−0.0110	−0.0094	−0.0077	−0.0059	−0.0040	−0.0021	0.0000	0.0022
0.40	−0.0115	−0.0100	−0.0084	−0.0067	−0.0049	−0.0030	−0.0011	0.0010	0.0031	0.0054	0.0077
0.45	−0.0093	−0.0077	−0.0060	−0.0043	−0.0024	−0.0005	0.0016	0.0037	0.0060	0.0083	0.0107
0.50	−0.0079	−0.0063	−0.0045	−0.0027	−0.0008	0.0012	0.0033	0.0055	0.0078	0.0102	0.0127
0.55	−0.0069	−0.0053	−0.0035	−0.0016	0.0003	0.0023	0.0045	0.0067	0.0091	0.0115	0.0141
0.60	−0.0062	−0.0045	−0.0027	−0.0009	0.0011	0.0032	0.0054	0.0076	0.0100	0.0125	0.0151
0.65	−0.0057	−0.0040	−0.0021	−0.0002	0.0018	0.0039	0.0061	0.0083	0.0107	0.0132	0.0158
0.70	−0.0053	−0.0035	−0.0017	0.0002	0.0023	0.0044	0.0066	0.0089	0.0113	0.0138	0.0164
0.75	−0.0049	−0.0032	−0.0013	0.0006	0.0026	0.0048	0.0070	0.0093	0.0118	0.0143	0.0169
0.80	−0.0046	−0.0029	−0.0010	0.0009	0.0030	0.0051	0.0073	0.0097	0.0121	0.0147	0.0173
0.85	−0.0044	−0.0026	−0.0008	0.0012	0.0032	0.0054	0.0076	0.0100	0.0124	0.0150	0.0176
0.90	−0.0042	−0.0024	−0.0006	0.0014	0.0035	0.0056	0.0079	0.0102	0.0127	0.0152	0.0179
0.95	−0.0040	−0.0023	−0.0004	0.0016	0.0036	0.0058	0.0081	0.0104	0.0129	0.0155	0.0181
1.00	−0.0039	−0.0021	−0.0002	0.0017	0.0038	0.0060	0.0082	0.0106	0.0131	0.0157	0.0183

From Table 2 the soil vertical speed trends are as follows: when the value of drill rotational speed (ω) is unchanged, the soil vertical speed (V_z) increases with the increase of the length of the rocker (l_{co}); when the value of the length of the rocker (l_{co}) is unchanged, the soil vertical speed (V_z) increases with the increase of the drill rotational speed (ω).   When the length of the rocker is greater than 0.7 m the drill rotational speed range ($V_z>0$) and takes the largest value.   Taking into account the size of the powered hole digger, the length of the rocker is determined as 0.75 m.

2.2   Overall structure of the powered new powered hole digger

The overall structure of the powered hole digger with slider-crank feeding mechanism is shown in Figure 2. The powered hole digger is mainly composed of a rack, a gasoline engine, a drill, belt pulleys, a reducer, a crank, a rocker and a support plate.   The gasoline engine, the large and small pulleys and the reducer are assembled and are fixed to the support plate.   The output shaft of the reducer, the crank and the rocker were connected and the other end of the rocker was connected to the support plate. The drill was connected to the output shaft of the gasoline engine which is connected with a small pulley.   The support plates are connected to guide rails by linear bearings and can reciprocate vertically as driven by the crank.   The power of the gasoline engine is dispersed into two parts at the output shaft: one part is transferred to the crank via the large and the small pulleys and the reducer and this portion drives the crank rotation and induces the drill to reciprocate vertically (vertical displacement of the drill).   The remaining power leads to the rotation of the drill.   The rotation of the drill together with the matching vertical reciprocation of the support plate facilitates the complement of the digging work. The main structural and performance parameters of the powered hole digger are shown in Table 3.
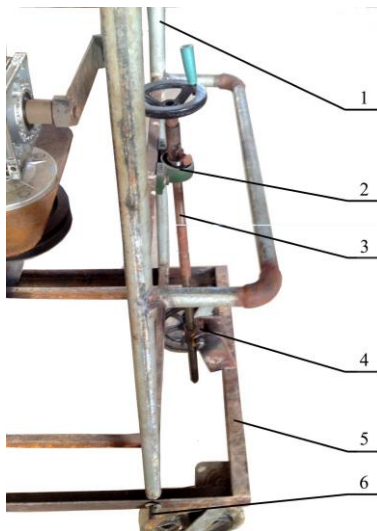

1. Upper rack   2. Rocker   3. Crank   4. Reducer   5. Big pulley   6. Small pulley   7. Lower rack   8. Drill 9. Gasoline engine   10. Support plate

Figure 2   Powered hole digger diagram

Table 3   Main structure parameters and operating parameters

Parameters	Values
Engine power/kW	3.5
The length of the crank/m	0.3
The length of the rocker/m	0.75
Starting position drill height from the ground/m	0.3
Hole depth/m	0.3
Drill total stroke/m	0.6

To meet the requirement of mountain digging operations, the upper and lower racks of this powered hole digger are hinged together.   There are four wheels which make contact with the ground mounted on the lower rack.   The rest of the machine is mounted on the upper rack.   The angle between the upper and lower racks can be adjusted by adjusting mechanism.   This research presents a digging angle adjustment - screw adjustment mechanism as shown in Figure 3.

1. Upper rack   2. Bearing   3. Screw   4. Nut   5. Lower Rack   6. Pin
Figure 3   Spiral adjustment mechanism

Screw adjustment mechanism is mainly composed of a screw and nut.   One end of the screw was fixed to the upper rack are fixed together by a bearing.   The nut and the lower rack are hinged together.   The screw is screwed into the nut and the upper rack and the lower rack hinged together by a pin.   When the screw is rotated, the angle between the upper rack and the lower rack is changed.

2.3   Motion characteristics analysis of slider-crank feed mechanism

2.3.1   Velocity (V_s) and displacement (S) of the slider

Let crank speed be ω_q then the angle between the crank and vertical line will be:

$$\beta = \omega_q t \qquad (4)$$

Solving simultaneous Equations (1), (2) and (4) to obtain (The actual speed of the crank is 0.33 rad/s):

$$V_s = \frac{\pi \sin(\frac{\pi t}{15})}{50} - \frac{\pi \sin(\frac{2\pi t}{15})}{50\sqrt{2\cos(\frac{2\pi t}{15}) + 23}} \qquad (5)$$

Differential equation of slider displacement is:

$$\begin{cases} \dfrac{dS}{dt} = V_s \\ S(0) = 0 \end{cases} \qquad (6)$$

Solving simultaneous Equations (5), (6) to obtain the slider displacement:

$$S = \frac{3\sqrt{2\cos(\frac{2\pi t}{15}) + 23} - 6\cos(\frac{\pi t}{15}) - 9}{20} \qquad (7)$$

Solving Equations (5) and (7) simultaneously and eliminating the parameter t to obtain drill feed rotational speed curve which was shown in Figure 4.
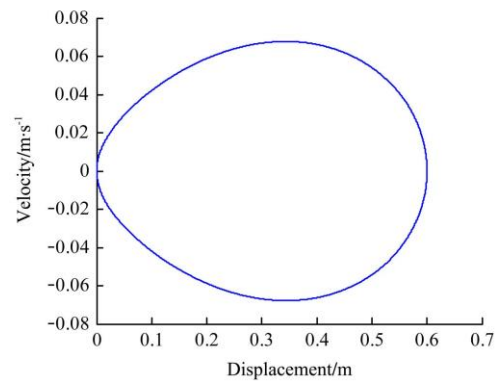

Figure 4   Feed speed curve of drill

Since the distance between drill and the ground is 0.3 m before the powered hole digger start to work, the actual start time of digging will not be t=0 s.   Let the start time of a work cycle of drill be t_0, the end time is t_1 to obtain an equation:

$$\begin{aligned} S(t_0) = 0.3 \\ S(t_1) = 0.6 \end{aligned} \qquad (8)$$

where, the solution is:

$$\begin{cases} t_0 = 8.4614 \text{ s} \\ t_1 = 15 \text{ s} \end{cases}$$

2.3.2   Parameter equation of the drill feed rate and the digging depth

The drill feed rate (f) is the distance the drill moves down on each rotation.   Feed rate (f) also equals to drill

feed distance (dS) in a period of time (dt) divided by number of turns of the rotation of drill (d$\varphi/2\pi$, dφ is the angle of rotating drill in a period of time (dt), dφ/d$t=\omega$). So the feed rate is:

$$f = \frac{dS}{\frac{d\varphi}{2\pi}} = \frac{V_s dt}{\frac{\omega dt}{2\pi}} = \frac{2\pi V_s}{\omega}$$

Substituting V_s and ω into the equation:

$$f = \frac{\pi \sin(\frac{\pi t}{15})}{150} - \frac{\pi \sin(\frac{2\pi t}{15})}{150\sqrt{2\cos(\frac{2\pi t}{15}) + 23}} \qquad (9)$$

Digging depth is derived as follows:

$$\begin{cases} h = s(t) - 0.3 \\ t_0 \leq t \leq t_1 \end{cases}$$

Substituting S (Equation (7)) into the equation:

$$\begin{cases} h = \dfrac{3\sqrt{2\cos(\frac{2\pi t}{15}) + 23} - 6\cos(\frac{\pi t}{15}) - 9}{20} - 0.3 \\ 8.4614 \leq t \leq 15 \end{cases} \qquad (10)$$

Solving Equations (9) and (10) simultaneously to obtain parameter equation of the drill feed rate and the digging depth.

$$\begin{cases} f = \dfrac{\pi \sin(\frac{\pi t}{15})}{150} - \dfrac{\pi \sin(\frac{2\pi t}{15})}{150\sqrt{2\cos(\frac{2\pi t}{15}) + 23}} \\ h = \dfrac{3\sqrt{2\cos(\frac{2\pi t}{15}) + 23} - 6\cos(\frac{\pi t}{15}) - 9}{20} - 0.3 \\ 8.4614 \leq t \leq 15 \end{cases} \qquad (11)$$

Eliminating the parameter t to obtain the curve of the drill feed rate changes with the drill digging depth which is shown in Figure 5.
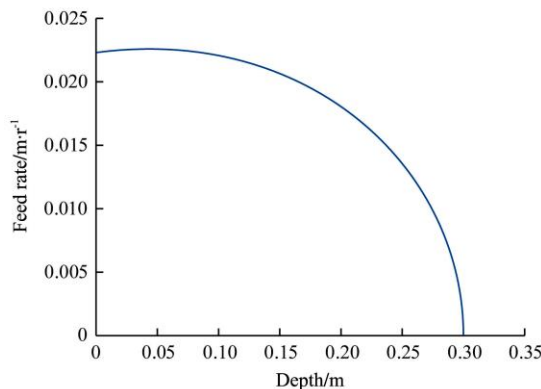

Figure 5   Drill feed rate curve

As shown in Figure 5, the drill feed rate increased when beginning and then decreased with digging depth increases.   After digging depth exceeds 0.2 m the drill feed rate decreasing gradients is greater.
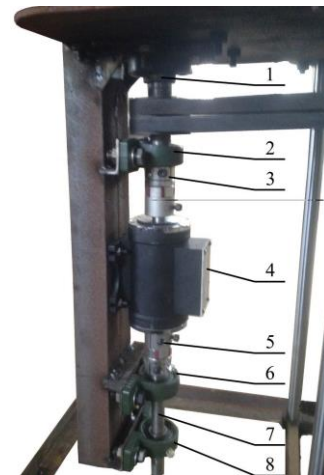
This objective of this research was to study the variation of drill power consumption in the mining process using the experimental method.

3   Power consumption test and data analysis

In this research, a torque meter (JN338-100A, Beijing New Century Aerospace Technology Co., Ltd.) was used to measure the time-varying speed and torque of the drill while digging, and the drill power data with varying pit depth was then calculated.

3.1   Design of experimental devices

The experimental device shown in Figure 6 was designed.   The power-output shaft of the gasoline engine was connected to one end of the torque meter through a coupling and the other end of the torque meter was connected to drill shaft via a coupling.   The drill was connected to the other end of the connecting shaft.   The drill shaft and the gasoline engine output shaft were fixed onto the rack through the bearing.   The torque meter was also connected on the rack.

1. Gasoline engine output shaft   2. Bearing   3. Coupling   4. Torque meter
5. Coupling   6. Bearing   7. Drill shaft   8. Bearing
Figure 6   Experimental device

3.2   Experimental methods

A flat land area at the Modern Agricultural Experimental Site in Huazhong Agricultural University was selected as the experimental site where a pit with a depth of 0.9 m, length of 1 m and width of 0.7 m was dug. The pit was filled with soil, then compacted ensuring the

thickness and humidity of each layer was consistent. Five (5) layers were created, each with a consistent thickness of 6 cm. The soil density of each layer is shown in Table 4. As shown in Table 4, the soil density of each layer is relatively constant while soil depth increases. Therefore it is assumed that the soil density did not affect the drill's power consumption significantly.

Table 4   Soil density of each layer

Layers	Soil density/kPa									
	1	2	3	4	5	6	7	8	9	10
1	53	45	53	45	45	45	45	53	53	53
2	45	45	53	60	53	53	53	53	53	53
3	49	55	54	53	48	53	53	45	49	45
4	53	53	45	53	45	53	53	53	53	53
5	53	53	53	53	53	45	45	53	53	45

Figure 7   Experimental site

Five test points were chosen within the selected area similar to the diagram shown in Figure 8. Experiments were carried out on these five points. Before the experiment, the powered hole digger was adjusted to ensure a vertically displaced drill. The torque meter was connected to a host computer with data acquisition card installed via a data cable. Additionally, the software was debugged to set the measurement interval and the measuring range. The experiment started when the engine was turned on. The drill bit was set at its highest point when data recording was started and the when the drill bit reached its lowest point the data recording stopped. During the entire course of digging operation, the engine throttle was adjusted to ensure smooth rotation of the drill. When each experiment trial was completed, the acquired data were saved and the drill was raised to

its highest position again, and made ready for the next test. Experimental data are shown in Figure 9.
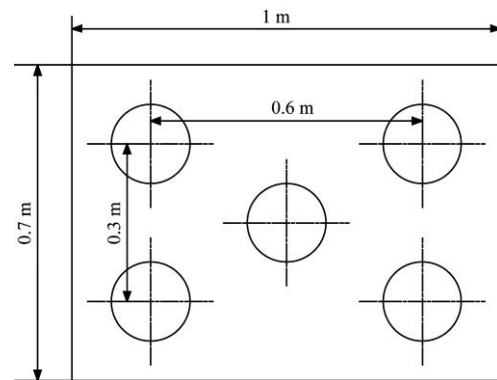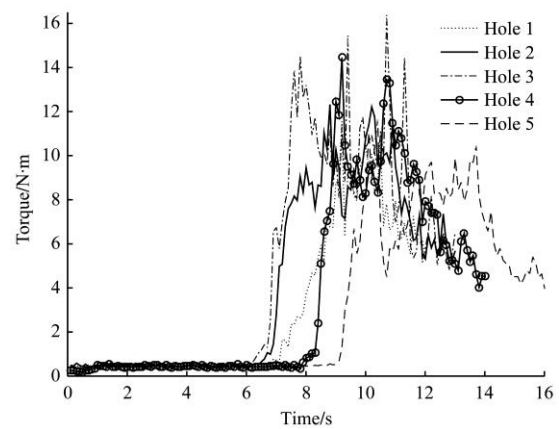

Figure 8   Points of the experiment

Figure 9   Torque

3.3   Data processing and analysis

Torque of each time point (T_i) times rotational speed of each time point (n_i) equals the drill power consumption of each time point (P_i). The interval between neighboring time points is ΔT_i. Drill rotational angle of each time point is φ ($\varphi=\sum n_i \times \Delta T_i$). The drill rotational angle of each time point can be converted to the displacement drill of each time point (S_i). Each S_i minus the drill spare travel equals digging depth of each time point (h_i). The drill power consumption of each drill digging depth is then calculated which are shown in Figure 10.

The data in Figure 10 were handled as follows: The abscissa (depth=[0, 0.3]) is equally divided into 30 segments, each segment with a length of 0.1 m. Find the average value of the abscissas and ordinates of all points in each segment (x_i, y_i). Find the standard deviation of the ordinates of all points in each segment then make new points whose abscissas and ordinates are x_i and y_i in the coordinate plane. A bar chart of those standard deviations is shown in Figure 11.
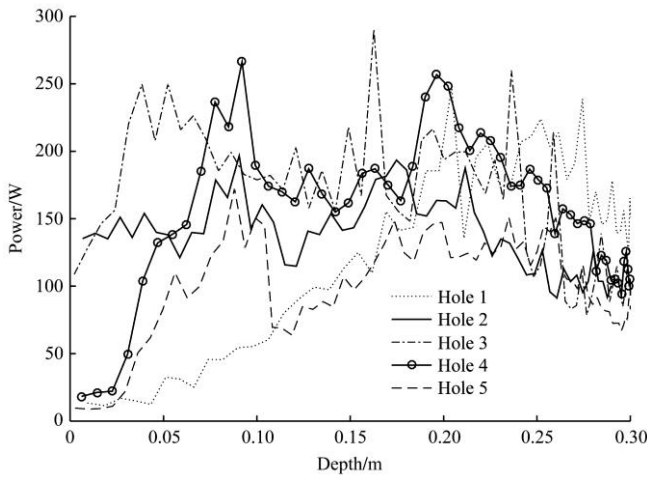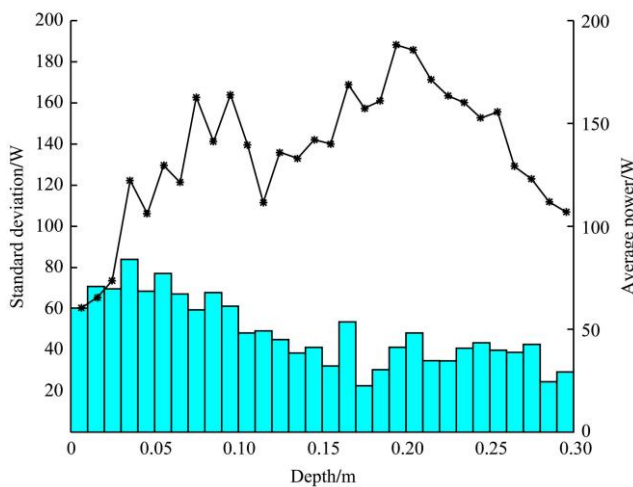
Figure 10   Power

Figure 11   Average power and standard deviation

As shown in Figure 11, the digging process is divided into three stages: initial stage (0-0.1 m), power up stage (0.1-0.2 m) and power down stage (0.2-0.3 m). The power consumption is very unstable in the initial stage. The data are very discrete in this stage. Digging became stabilized in the stage where the digging depth was beyond 0.1 m. The drill power consumption showed an increasing trend in the power up stage. Power consumption reached the maximum on the point that the digging depth is 0.2 m. The drill power consumption showed a decreasing trend in the power down stage.

The reasons would include: Since the soil affects the drill, the rotational speed and feed speed of the drill are suddenly reduced when the drill initially meets the soil surface, while the torque of the drill suddenly increases; at this time the drill power consumption starts to increase. When the drill torque decreases, the rotational speed and the feed speed of drill increases and the drill power consumption starts to decrease. Consequently, the feed rate of drill decreases rapidly in the stage that the digging depth is beyond 0.2 m. The drill power consumption decreases with the increase of digging depth in this stage.

4   Discussion and conclusions

1) The maximum slider feed speed which corresponds to different rocker lengths is determined in this way: The discrete rocker length and discrete crank rotation angle are substituted into a slider instantaneous center radius expression. In order to design a slider-crank feed mechanism which meets the need, a suitable rocker length is determined according to transport soil theory.

2) The relationship between drill feed speed and drill displacement and the relationship between the drill feed rate and the digging depth are expressed in the form of parametric equations. Curves are drawn. The drill feed rate decreases with the increase of digging depth in the latter stages of the digging process.

3) Characteristic experiments to obtain the power consumed by the drill were conducted. Time-varying power was converted into discrete digging depth power consumption proportions and a total cumulative power ascertained; how the digging depth varied with the amount of power consumed was analyzed via a segmented calculation method. A positive correlation between the drill power consumption and the powered hole digger's feed rate was found.

4) The results of this experiment were obtained and were valid in cases where the soil density of each layer remained relatively consistent. In real-world conditions the soil density increases with the deepening of digging depth, so drill working resistance will increase. The feed rate of the powered hole digger using a slider-crank feed mechanism is gradually reduced, therefore the powered hole digger will work smoothly and is not expected to stall.

[References]

[1] Zhuo F. Digging Machine. Beijing: China Forestry Publishing House, 1989. pp.56–121. (in Chinese)

[2] Kathirvel K, Job T V, Karunanithi R, Swaminathan K R. Development of auger digger as attachment to power tiller. AMA, Agricultural Mechanization in Asia, Africa and Latin America, 1990; 21(4): 9–10.

[3] Singh R D. Performance of a simple tractor-mounted deep-hole digger. AMA, Agricultural Mechanization in Asia, Africa and Latin America, 1982.

[4] Purtskhvanidze M, Keller N. Hole digger for slopes. Sel'skiĭ Mekhanizator, 1990.3.

[5] Wang N, Liu H. Effects of working parameters on dynamic mechanical parameters for digging machine (I). Test and study of dynamic mechanical parameters for digging machine. Journal of Beijing Forestry University, 2002; 24: 195–199. (in Chinese with English abstract)

[6] Ma Y. Study on pit-shaping control of tree-planting machinery and computational method of pit-digging resistance. Journal of Dynamics & Control, 2007; 3: 267–270.

[7] Meng Q. Research on simulation and mathematical interpretation of dynamic process to earth auger for tree deep planting. Northeast Forestry University, 2007. (in Chinese with English abstract)

[8] Yang Y G, Liu Y C. The theory evaluation and the experimental verification of the special pair of hole digger flexural vibration. Transactions of the CSAM, 1997; 28(2): 51–55. (in Chinese with English abstract)

[9] Yang Y G, Liu Y C, Lü X M. Dynamic analysis of torsional vibration for a hole digger. Transactions of the CSAM, 2005; 36(9): 53–67. (in Chinese with English abstract)

[10] Macpherson J D, Jogi P N, Kingman J E E. Application and analysis of simultaneous near bit and surface dynamics measurements. SPE Drilling & Completion, 2001; 16(4): 230–238.

[11] Brakel J D, Azar J J. Prediction of wellbore trajectory considering bottomhole assembly and drill-bit dynamics. SPE Drilling Engineering, 1989; 4(2): 109–118.

[12] Engin S, Altintas Y. Mechanics and dynamics of general milling cutters. Part I: helical end mills. International Journal of Machine Tools & Manufacture, 2001; 41(15): 2195–2212.

[13] Engin S, Altintas Y. Mechanics and dynamics of general milling cutters. Part II: inserted cutters. International Journal of Machine Tools and Manufacture, 2001; 41(15): 2213–2231.

[14] Altintas Y, Shamoto E, Lee P. Analytical prediction of stability lobes in ball end milling. Journal of Manufacturing Science and Engineering, 1999; 121(4): 586–592.

[15] Altintas Y, Engin S. Generalized modeling of mechanics and dynamics of milling cutters. CIRP Annals-Manufacturing Technology, 2001; 50(1): 25–30.